Chapter 4

Redox sensitive TPGS-SH NP

4. Redox sensitive TPGS-SH nanoparticles for lung cancer therapy

4.1. Objective of the study

The objective of the current study was the development, optimization and preparation of cetuximab conjugated novel redox sensitive thiolated nanoparticles of docetaxel and to evaluate their physicochemical, *in-vitro* release characteristics, *in-vitro* cellular uptake, cytotoxicity, apoptosis and wound-healing studies on A549 cells, pH and redox sensitivity, *in-vivo* pharmacokinetics, histopathology studies in rats and *in-vivo* efficacy in B(a)P induced lung cancer mice model after *i.v.* administration.

4.2. Plan of study

a. Preparation docetaxel loaded redox sensitive thiolated nanoparticles using modified dialysis method

b. Post-conjugation of cetuximab on the surface of docetaxel loaded redox sensitive thiolated nanoparticles

c. Evaluation of redox sensitive nanoparticles

- Particle size, polydispersity index and zeta potential by DLS
- Electron microscopy (SEM, TEM & AFM)
- Determination of entrapment efficiency
- pH and redox sensitivity studies
- *In-vitro* drug release studies in two different buffers (pH 5.5 & pH 7.4) with different GSH concentrations (5,10 and 20 mM)
- *In-vitro* cytotoxicity, apoptosis and wound healing studies on A549 cells
- *In-vitro* stability of nanoparticles on lyophilization and reconstitution, plasma and serum incubation and storage stability

- *In-vivo* histopathology study on rats
- *In-vivo* anticancer efficacy studies on B(a)P induced lung cancer mice model

4.3. Material

Docetaxel (99.56% pure) was a generous gift from Neon Labs. Cetuximab (Erbitux®) was arranged by Merck Specialities Ltd, Mumbai. TPGS was a liberal gift from Isochem, France. 4-amino thiophenol (4-ATP), 4-dimethyl aminopyridine (DMAP), 1 -ethyl-3-(3-dimethylaminopropyl) carbodiimide (EDC) and N-hydroxysuccinimide (NHS), dialysis membrane one kDa were purchased from Sigma Aldrich, CA, USA. 3-(4,5-Dimethylthiazol-2-yl)-2,5-diphenyltetrazolium bromide (MTT) was supplied by SRL, Mumbai. Cell culture media, buffers were obtained from Hi-media labs, Mumbai, India. Antibiotic-antimycotic (penicillin-streptomycin) and trypsin-EDTA were procured from Genetix Biotech Asia, Mumbai, India. Phalloidin-tetramethyl rhodamine conjugate was purchased from AAT Bioquest Inc. USA. All other chemicals were of analytical grades.

4.4. Methods

In the development of DTX loaded redox sensitive nanoparticles (NPs), Quality by Design (QbD) was employed which is a proactive, modern and scientific approach to product design and development [187,188].

4.4.1. Cause–effect relationship: Ishikawa fishbone

A risk assessment study and the cause-effect relationship between the factors responsible and the critical quality attributes (CQAs) were configured by employing the Ishikawa fishbone diagram (figure 4.1) [189-191]. With existing knowledge and expertise, particle size (PS), zeta potential (ZP), and entrapment efficiency (EE) were selected as key CQAs in the present study [192,193].

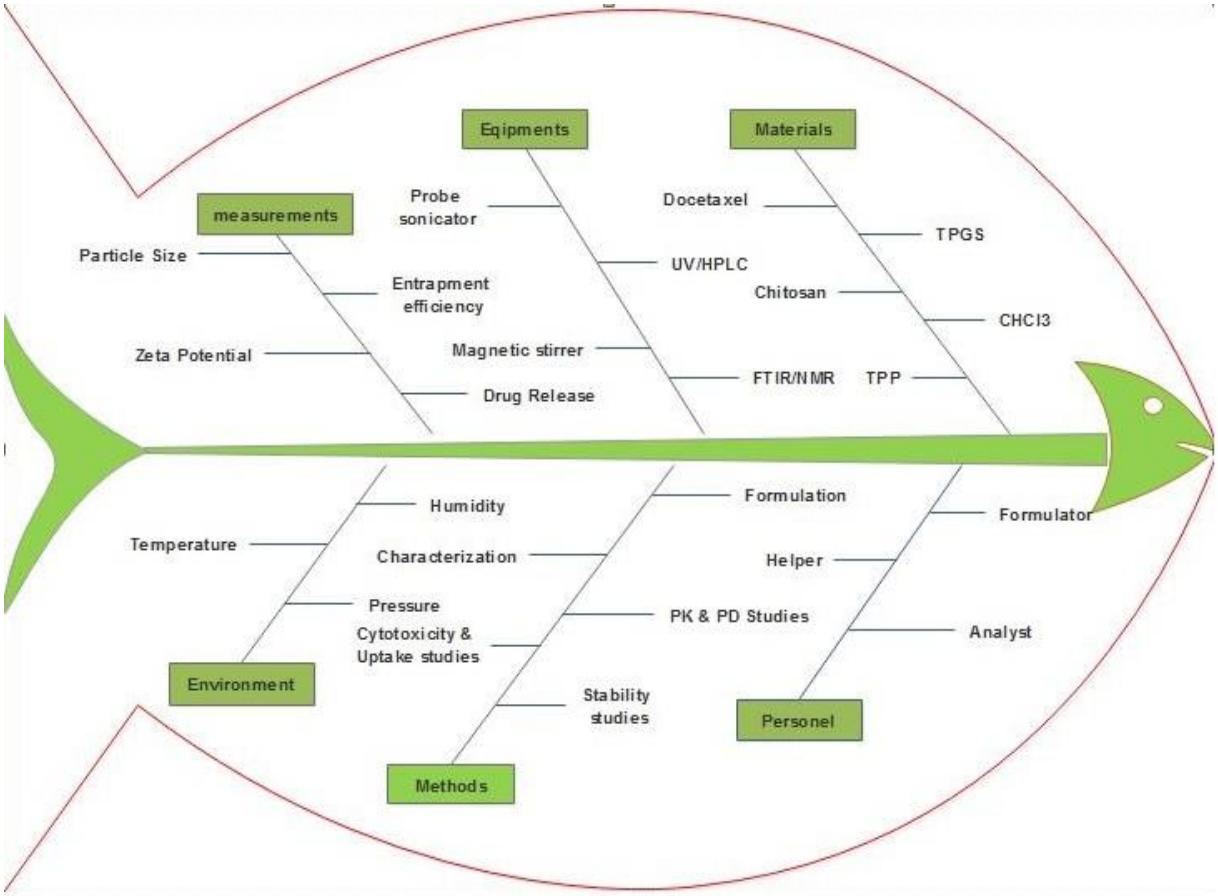

Figure 4.1. Ishikawa fishbone diagram showing the cause-effect relationship between variables for the critical quality attributes of DTX loaded redox sensitive nanoparticles

4.4.2. Risk assessment: Plackett–Burman design

The significant effect of identified risk factors on the mentioned CQAs was evaluated by Plackett–Burman design (PBD). The screening experiments with four factors and three CQAs were performed initially with the highest and lowest levels of factors. PBD was constructed using Minitab 19 software (Minitab, Inc., PA, USA), followed by statistical analysis (table 4.1) [194,195]. From the said experimental design, the observed CQA values were enlisted in table 4.1. The significance of PBD and the coefficients for each factor were evaluated by applying analysis of variance (ANOVA). Further, the key factors that influence CQAs (responses) on a large scale were selected by employing the Pareto charts (figure 4.2) [196,197].

Table 4.1. Composition of docetaxel loaded redox sensitive NP with the levels of various factors and the results of observed mean values of various responses by Plackett–Burman design. & List of the selected three factors and their levels for the 3^3 factorial design along with the responses

Run	PC	T	SS	DD	PS	EE	ZP
PBD-1	40	10	200	12	289±11.5	70.23±5.6	21.26±1.12
PBD-2	10	10	50	12	245±12.7	63.27±5.1	16.59±1.47
PBD-3	10	40	200	36	278±13.4	61.01±3.7	14.35±0.98
PBD-4	40	40	50	36	384±21.6	69.95±4.9	17.71±1.42
PBD-5	10	10	200	36	216±12.1	60.08±5.2	13.01±0.84
PBD-6	40	40	200	12	354±19.2	68.11±4.7	15.74±0.96
PBD-7	10	40	50	12	231±13.9	62.84±5.8	13.14±1.18
PBD-8	10	10	50	36	195±13.8	64.19±3.5	16.17±1.45
PBD-9	40	40	50	36	364±26.1	68.47±5.3	16.97±0.99
PBD-10	40	10	200	36	331±26.4	69.03±3.2	18.45±1.02
PBD-11	40	10	50	12	346±22.3	71.33±5.4	23.56±1.93
PBD-12	10	40	200	12	257±16.7	60.98±3.8	13.67±0.71

Independent Variables (factors)	Name	Unit	Minimum	Maximum
X1	Polymer Concentration	mg/10 ml	10	50
X2	Temperature	℃	10	40
X3	Stirring speed	RPM	50	200
Dependent Variables (responses)	**Name**	**Unit**	**Constraint**	
Y1	Particle Size	nm	Minimize	
Y2	Entrapment Efficiency	%	Maximize	
Y3	Zeta Potential	mV	Maximize	

PC-Polymer concentration
T-Temperature
SS-Stirring speed
DD-Duration of dialysis
PS-Particle size
EE-Entrapment efficiency
ZP-Zetapotential

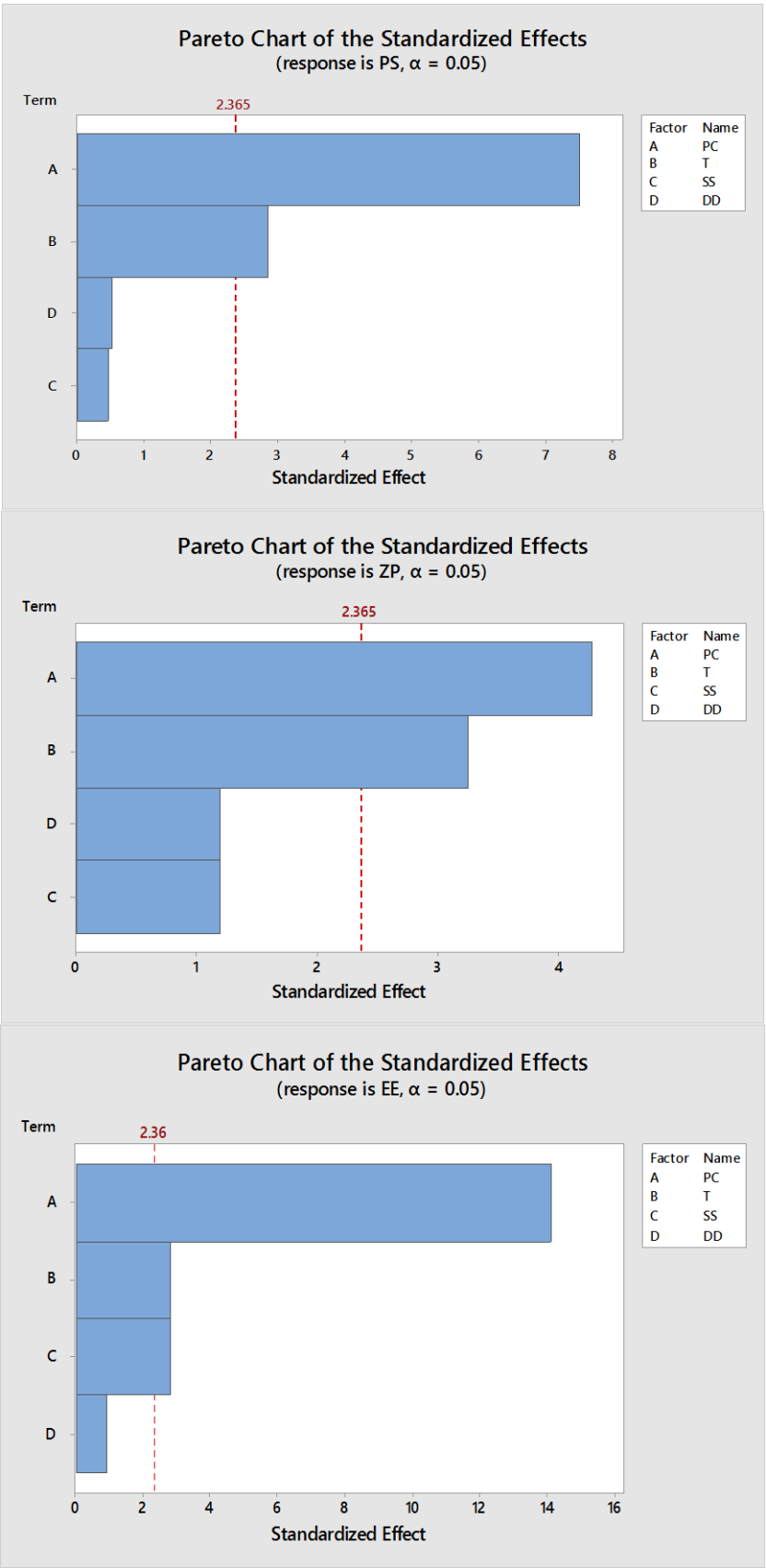

Figure 4.2. Pareto charts showing the influence of factors on responses (particle size, zeta potential and percentage entrapment efficiency) of DTX loaded redox sensitive NP.

4.4.3. Optimization of nanoformulation: 3^3 factorial design

The effect of three main factors (polymer concentration [PC], temperature [T], and stirring speed [SS]) on the critical responses (PS, ZP, and EE) was evaluated. A 3^3 factorial design (FD; 3-factor, 3-level) was applied to optimize the redox sensitive TPGS-SH NP(table 4.2) in terms of the small size with narrow distribution; higher surface charge for better stability and efficient drug loading to reduce the dose and related side effects [198]. The experimental design was constructed and evaluated by using Minitab 19 software. Fifteen batches were prepared as per FD and their compositions were presented in Table 4.2. To determine the significance of the experimental model, ANOVA was employed [199].

The polynomial equation generated by FD, elucidating the effect of factors on each of the responses is as follows:

$$Y_r = \delta_0 + \delta_1 X_1 + \delta_2 X_2 + \delta 3 X_3 + \delta_{12} X_1 X_2 + \delta_{13} X_1 X_3 + \delta_{23} X_2 X_3 + \delta_{123} X_1 X_2 X_3$$

4.4.4. Synthesis of thiolated TPGS (TPGS-SH)

To synthesize the TPGS-SH, EDC and NHS were used initially to bring about the reaction between the carboxylate groups located on the TPGS with the primary amine of 4-amino thiophenol (4-ATP) by carbodiimide chemistry [228].

The NHS and EDC, at a ratio of 1:2 (i.e., TPGS-COOH to EDC (or NHS) at 1:2 molar), were added into TPGS-COOH. This mixture was stirred mildly at pH 5 and 25 °C for 3 h; the ethanolic solution of 4-ATP (10 ml), at a molar equivalence of 1:1 (4-ATP: TPGS-COOH), was transferred to above reaction mixture and stirred in the dark overnight at 4 °C under N_2 atmosphere so as to avoid oxidation of thiol groups. The pH was once again brought to 7 using sodium borohydride that can circumvent the disulfide bonds. The

precipitation was carried out using ethyl alcohol. The final pure solution was then lyophilized. The light yellow product of thiolated TPGS was collected [228,229].

Table 4.2. The 3^3 factorial design matrix and results of observed mean values of various responses & The predicted and the actual values of the selected responses considered for optimized formulation FD-14

Run order	**X_1**	**X_2**	**X_3**	**Y_1 ***	**Y_2***	**Y_3***
FD-1	30	25	100	208.87±9.59	73.94±3.51	26.47±1.12
FD-2	30	10	50	227.94±13.01	66.47±4.07	18.92±0.85
FD-3	30	40	50	191.36±8.76	65.62±5.78	15.78±0.99
FD-4	10	25	50	199.34±10.45	61.25±2.76	17.31±0.74
FD-5	10	10	100	201.61±9.91	60.79±4.97	13.77±0.81
FD-6	30	40	200	218.45±12.43	67.51±2.43	16.96±0.96
FD-7	30	25	100	224.55±10.82	70.86±5.22	26.85±1.54
FD-8	50	10	100	219.78±10.06	68.67±5.84	19.63±1.02
FD-9	50	25	50	227.38±8.43	67.48±3.05	17.42±1.03
FD-10	50	25	200	231.71±10.67	68.11±3.31	20.44±1.23
FD-11	50	40	100	229.85±9.19	69.28±4.75	13.69±0.82
FD-12	10	40	100	189.49±8.13	63.75±2.61	11.95±0.58
FD-13	30	10	200	205.91±9.05	65.44±2.08	18.35±1.09
FD-14	30	25	100	209.42±11.75	74.14±3.92	27.88±1.50
FD-15	10	25	200	195.56±9.04	62.73±1.99	14.61±0.47

Selected factors for optimization of responses		
Independent Variables (Factors)	**Results obtained from Factorial Design**	
X1-Polymer Concentration (mg)	30 mg	
X2-Temperature (℃)	25 ℃	
X3-Stirring speed	100 rpm	
Dependent Variables (Responses)	**Predicted value**	**Observed value**
Y1-Particle Size (nm)	209.42±11.75	227±8.219
Y2-Entrapment Efficiency (%)	74.14±3.92	71.08±1.016
Y3-Zeta Potential (mV)	27.88±1.50	22±1.054

Table 4.3. Formulation of different redox sensitive TPGS-SH NP

Formulation	DTX (mg)	CM6 (mg)	TPGS-COOH (mg)	TPGS-SH (mg)	CTX (mg)
Simple redox sensitive TPGS-SH NP	**3**	--	--	**30**	--
CM6 loaded non-targeted redox sensitive TPGS-SH NP	--	**3**	**10**	**20**	--
CM6 loaded targeted redox sensitive Np	--	**3**	**10**	**20**	**2.5**
Non-targeted redox sensitive TPGS-SH NP	**3**	--	**10**	**20**	--
Targeted redox sensitive TPGS-SH NP	**3**	--	**10**	**20**	**2.5**

4.4.5. Chemical characterization of TPGS-SH

The prepared TPGS-SH was characterized by FTIR spectroscopy and ^{1}H and ^{13}C NMR spectroscopy [230].

4.4.6. Preparation of redox sensitive nanoparticles (redox sensitive NP)

Different batches of redox sensitive NP were prepared by modified dialysis method as per table 4.2 and same was depicted in figure 4.3. Briefly, docetaxel (DTX) or coumarin-6 (CM6) were dissolved in a DMSO solution of TPGS-SH (30 mg). The resulting solution was dialyzed against distilled water for 24 h. After the specified time, the formed NP were separated from the suspension by centrifugation at 17000 rpm, washed with distilled water three times and resuspended in distilled water. The targeted NP were formed by a similar procedure except that in place of 30 mg of TPGS-SH, a mixture of TPGS-SH and TPGS-COOH (20 and 10 mg respectively) was used. Surface conjugation of cetuximab was accomplished with EDC/NHS system (1:5) which activates carboxylate groups on NP surface. Following, cetuximab (2.5 mg) was added to the NP suspension and again

stirred for 30 min. The resulting formulation was subjected to dialysis against DTX saturated solution using 1kDa membrane to remove unentrapped drug and reactants [231].

4.4.7. Evaluation of physicochemical characteristics of NP

4.4.7.1. Particle size and polydispersity index

Particle Size and polydispersity were determined by dynamic light scattering (DLS) principle in a Malvern Zetasizer Nano S-90. The measurements were taken without dilution of NP suspension [26].

4.4.7.2. *Zeta potential measurement*

Zeta potential of NP was measured by zetasizer (Nano ZS, Malvern Instruments, Malvern, UK). Following appropriate dilution of samples, the formulations were scanned for the surface charge measurements. Zeta potential measurement will determine the influence of surface charge on the stability of NP [232].

4.4.7.3. Electron microscopy (SEM & TEM)

Study of the external morphology (particle size and the shape) of redox-sensitive TPGS-SH NP was done using transmission electron microscopy (TEM) and scanning electron microscopy (SEM) [233].

4.4.7.4. Surface texture by atomic force microscope (AFM)

The surface texture of DTX loaded redox sensitive TPGS-SH NP was realized by AFM at normal temperature and pressure and by keeping the instrument under tapping state. The NP suspensions were sufficiently thinned with ultrapure water and tiny drops were then placed on the glass coverslips. These coverslips were then dried under vacuum at 25 °C for 24 h. The AFM data were analyzed by AFM image analysis software [233].

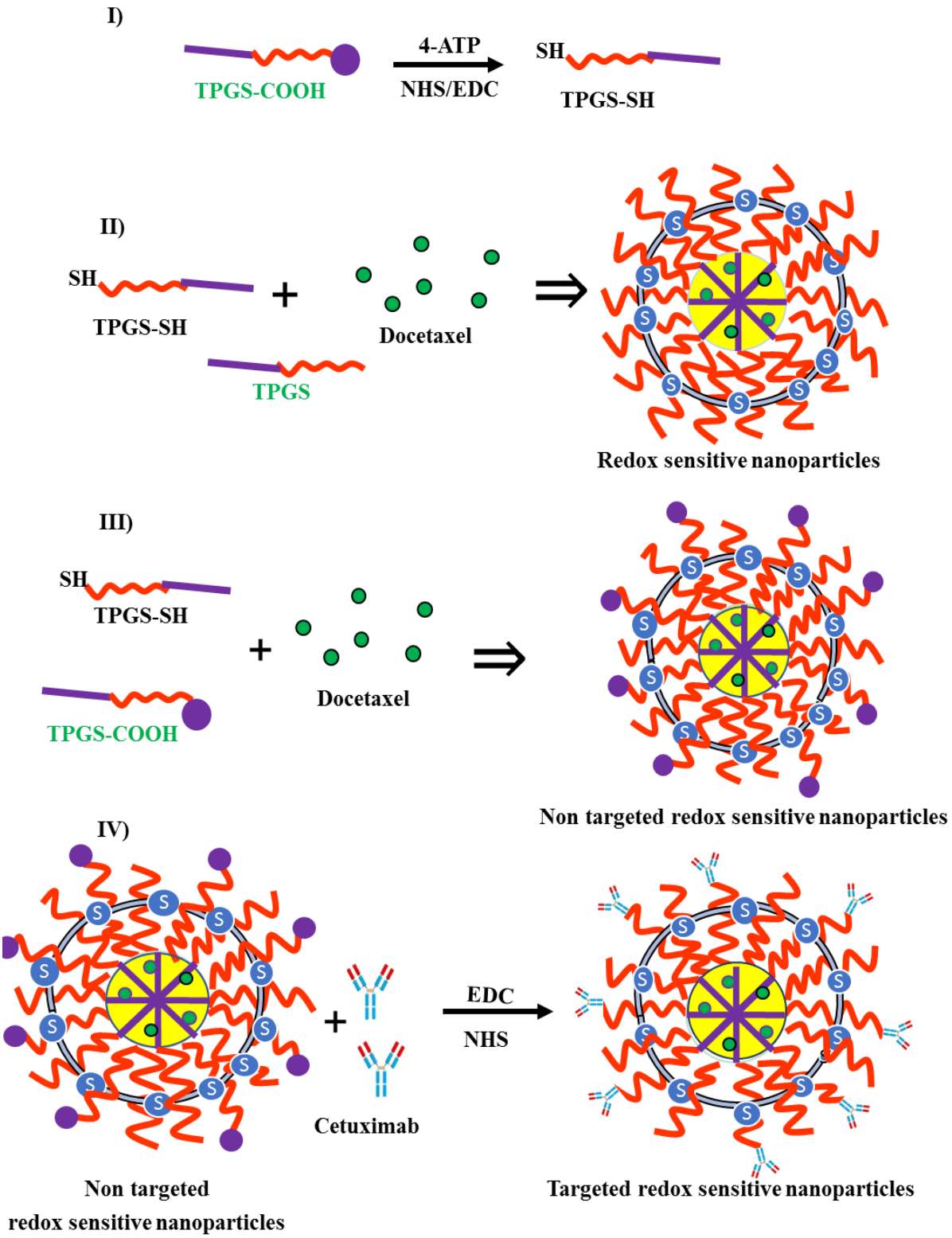

Figure 4.3. Scheme for the preparation of targeted redox sensitive NP

4.4.7.5. Entrapment efficiency (EE)

Drug loaded redox sensitive TPGS-SH NP (0.1 ml, ~300µg) were dissolved in a solvent system comprising a 50:50 mixture of acetonitrile and deionized water (10 ml). The resulting solution was passed through a 0.45 µm membrane filter and absorbance was determined using RP-HPLC at 230 nm [234].

EE was calculated as: $EE\ (\%) = \frac{\text{Docetaxel entrapped in the NP}}{\text{Docetaxel added in the NP preparation process}} \times 100$

4.4.7.6. Evaluation of CTX concentration

The final concentration of CTX in the prepared targeted redox sensitive NP was realized by Bradford assay [175]. For this, 1ml of each targeted NP and blank PBS pH 7.4 and standard CTX solution were made to react for 5 min with 5 ml Bradford reagent separately and the corresponding UV absorbances were measured. The total amount of CTX conjugated onto the targeted redox sensitive NP was then derived from the calibration curve of bovine serum albumin (BSA). The equation to assess the degree of conjugation was

$$\text{Extent of CTX conjugation} = \frac{\text{CTX amount in targeted redox sensitive NP} - \text{CTX amount in blank (PBS)}}{\text{amount detected in standard CTX solution}}$$

4.4.8. In-vitro studies

4.4.8.1. Drug release study

The release kinetics of DTX from TPGS-SH redox sensitive NP were studied in two types of buffers, i.e., pH 5.5 and 7.4, which contain different concentrations of GSH (5 mM, 10 mM and 20 mM) to mimic the intracellular reductive environment. Drug-loaded NP suspension, in respective GSH containing buffer, was placed in the dialysis bag (cellulose membrane, 1kDa) and sealed tightly with dialysis clips and then immersed into receptor

medium of same buffer (50 ml). By continuously stirring at 100 rpm, the whole set up was maintained at 37 ± 0.5 °C. Sample collection (15 ml) was performed, at predetermined time periods, from the receptor compartment and the same volume of fresh medium was added to the receptor compartment. Docetaxel has insignificant solubility in phosphate-buffered saline (pH 7.4). Therefore, the addition of 0.1% w/v Tween 80 to the receptor compartment can maintain proper sink condition. The extent of drug release was determined by RP-HPLC at 230 nm [235].

4.4.8.2. pH/redox sensitivity studies

The pH sensitivity of prepared redox sensitive NP was studied by storing the formulations at different pH conditions (pH 2, 3, 4, 5 and pH 7) for 24 h at 37 °C and then measuring the change in particle size by DLS. Similarly, the redox sensitivity was realized by incubating the NP suspensions with different GSH concentrations (5mM, 10mM and 20 mM) for 24 h followed by measuring the change in particle size by DLS [228,236].

4.4.8.3. Cellular uptake study

To assess the extent of cell uptake of NP, A549 cells were separately seeded, at a density of 50,000 cells per well, into a 6-well plate and allowed for proper cell adhesion for 24 h. Following, free CM6, CM6 loaded nontargeted and targeted redox sensitive NP were added to different wells and plates were kept in the incubator for at least 2 h. Pre-treatment was done with CTX to one of the wells before incubation with targeted redox sensitive NP, so as to confirm the definitive role of EGFR in intra-cellular uptake of NP. The spent medium containing treatments was removed and treated cells were irrigated thrice with 1ml PBS. The washed cells were then fixed with 4% paraformaldehyde and stained with DAPI, kept aside for 15 min. The stained cells were finally imaged with a fluorescence microscope (EVOS® FL Imaging System, Life Technologies, California) [174].

4.4.8.4. Cytotoxicity study

The cytotoxicity of the prepared redox sensitive NP and Docel^{TM}, on A549 human lung carcinoma cells, was evaluated by MTT assay. For this, A549 lung cancer cells were plated into 96 well plate and subsequent incubation, for 12 h, was done to facilitate the appropriate cell adhesion. The cells were then incubated with redox sensitive formulations and Docel^{TM} in DMEM at various dilutions (0.025, 0.25, 2.5 and 25 µg/ml of DTX) for 24 h. Following, treatments were removed and cells were washed with PBS. 100 µl fresh DMEM along with 10 µl of MTT in PBS (5mg/ml) was then added to each well. Again, incubation was done for 2 h after which, the spent medium along with MTT was discarded. The wells were added with 100 µl of DMSO and the plates were shaken gently on a gyratory shaker for 5 min to dissolve formazan crystals. The optical density was then computed at 570 nm using microplate reader. Cytotoxicity was assessed for the treated cells with respect to untreated cells [237]. The % cell viability was determined as

Cell viability (%) = (Absorbance from treated cells/Absorbance from control cells) x 100

4.4.8.5. Cellular apoptosis study

For this study, A549 cells were added into 6-well plates containing coverslips at a count of 50,000 cells per well and incubated for 24 h. Cells were then added with Docel^{TM,} nontargeted and targeted redox-sensitive NP at their respective IC_{50} concentrations obtained from *in-vitro* cytotoxicity study along with medium as control and then placed in the incubator for 6 h. After routine fixing with paraformaldehyde, DAPI staining for 5 min followed by phalloidin tetramethyl rhodamine conjugate counterstaining in PBS along with 1% BSA at room temperature for another 30 min were done respectively. The stained cells were then washed with coldish PBS for 3 times [238,239]. Following, the

coverslips were taken out from wells and placed on glass slides and imaged with the fluorescence microscope (OLYMPUS, IX 71, Japan).

4.4.8.6. Wound-healing assay

Wound-healing assessment was carried out to reckon the extent to which cells migrate by observing the movement of cells into and then cover an acellular space post wounding. A549 cells, after forming into monolayers, were scratched as straight as possible with a 1 ml pipette tip to create an acellular space. The wells were then irrigated thrice with PBS (pH 7.4) and then added with media containing Docel^{TM}, non-targeted and targeted redox sensitive NP and plain DMEM as control. Following incubation at 37 °C for 48 h, the extent of cell migration was assessed with inverted microscope (Olympus CKX41) after 6, 12, 24 and 48 h [240,241].

4.4.9. Stability studies

The prepared redox sensitive TPGS-SH NP were evaluated for their stability in terms of change in their particle size, polydispersity and zeta potential and entrapment efficiency before and after lyophilization, incubation with serum and plasma (4h & 12h respectively) and also effect of storage for six months. Briefly, the prepared targeted redox sensitive formulations were freeze-dried after the addition of suitable cryoprotectant and their particle size and other parameters were measured before and after freeze-drying. Also, prepared formulations were incubated with equal volumes of rat plasma and serum for specified time and then evaluated for above parameters. Finally for storage stability, the targeted formulation was lyophilized, sealed in air-tight amber colored glass vials and stored (4 °C). At predetermined time points, samples were withdrawn from the vials, reconstituted and the same were analyzed for the above mentioned parameters, in order to ascertain their storage stability [232,242].

4.4.10. In-vivo studies

4.4.10.1. Pharmacokinetics studies of NP in rats

The Charles Wistar rats (150-200g) were randomly segregated into four groups, with six rats in each group (n=6). Group 1 received an intravenous (i.v.) injection (via lateral tail vein) of Docel™ while Group 2 and Group 3 were injected i.v. with non-targeted and targeted redox sensitive TPGS-SH NP, respectively. Group 4 received saline to serve as negative control. Totally 24 rats were used for this study. Rats were monitored for health, motor activity, stress, illness and associated mortality on a regular basis. At predetermined intervals (0.5, 1, 2, 4, 8, 12, 24 and 48 h) rats were anesthetized (urethane 2 gm/kg intraperitoneally) and blood samples were collected (via tail vein) from all rats.

For pharmacokinetic analysis, the samples were vigorously stirred and the drug was extracted using an organic solvent. After that, the mixture was centrifuged and the supernatant organic layer was separated for drying. Then, the dried residue was reconstituted in the mobile phase, vortexed and the solutions were again centrifuged. Finally, solutions were injected into the RP-HPLC column under suitable flow rate. The column effluent was sent to a UV-VIS detector for analysis at 230 nm. The quantity of DTX was then computed from the calibration curve constructed previously using blank blood containing different concentrations of standard DTX. Pharmacokinetic parameters were calculated using the Kinetica® software [243,244].

4.4.10.2. Histopathology studies

After administration of saline, Docel™, redox sensitive formulations (multiple dosing at 7.5 mg/kg) to separate groups of rats, once in every three days and for 3 times, animals were euthanized on 15th day and then the vital organs like lungs liver, kidneys and heart were collected and washed with normal saline. Regular fixing with 10% formalin

followed by paraffin blocking were done. After routine processing, paraffin sections of 5 µm thickness were mounted on separate glass slides. The above sections were treated with haematoxylin & eosin (HE) for cytoplasmic contrast microscopy and then visualized under microscope for histopathological findings [245,246].

4.4.10.3. Evaluation of anticancer efficacy of nontargeted and targeted formulations

The Swiss albino mice were segregated into five groups with each group consisting six mice. Group I was designated as negative control and was administered with peanut oil orally for four weeks. Group II animals were treated with benzo(a)pyrene ((B(a)P) 50 mg/kg body weight dissolved in peanut oil orally) weekly twice for 4 weeks, to induce lung cancer by 16th week, which serve as model control. Group III and IV animals were treated with non-targeted and targeted TPGS-SH redox sensitive NP (i.v., 7.5 mg DTX/kg body weight) for 4 weeks after they were treated with the first dose of B(a)P (as in Group II). The induction of lung cancer was confirmed by histopathological evaluation. Group V animals were treated with Docel^{TM} for 4 weeks after they were administered with first dose of B(a)P. Food and water will be available *ad libitum*. During the study, the health conditions of mice were monitored every day, and the body weights were measured every week. Survival analysis was done by applying Kaplan-Meier survival curves to compute percent survival (Liu et al., 2013). After 16 weeks, the mice were anesthetized and then sacrificed [247-249]. Subsequently, the lungs were dissected, fixed with 10% formalin and then paraffin blocking was done. After routine processing, paraffin sections of a 5 µm thickness were mounted on separate glass slides. The above sections were treated with hematoxylin & eosin (HE) and these sections were analyzed for cancer cell numbers by using ImageJ software [250-253].

4.4.11. Statistical evaluation

All values presented were average of three individual measurements along with standard deviation. One-way ANOVA was employed to compute the significant differences and $p<0.05$ was considered as statistically significant.

4.5. Results and discussion

4.5.1. Risk identification & risk assessment screening

From risk assessment studies, PC, T, and SS were identified as significant variables that influenced the responses through preliminary screening by PBD (table 4.1) and; PS, ZP and EE were selected as responses (table 4.1). Pareto charts for PS, ZP, and EE are shown in figure 4.2. ANOVA was employed to evaluate the significance of PBD and statistically significant coefficients for each factor.

4.5.2. 3^3 Factorial design

The mean PS of the optimized nanoformulation developed according to the 3^3 FD was in the range of 189.49±8.13 nm to 231.71±10.67 nm (table 4.2). The polynomial equation generated by the FD showing the effect of factors on PS was as follows:

Particle size =

164.8 + 3.589 PC + 1.367 T - 0.0444 SS + 0.319 DD

The ZP of the optimized nanoformulation developed according to the 3^3 FD was in the range of 11.95±0.58 mV to 27.88±1.50 mV (table 4.2). The polynomial equation generated by the FD showing the effect of factors on ZP is as follows:

Zeta potential =

17.56 + 0.1389 PC - 0.1056 T - 0.00778 SS - 0.0486 DD

The EE of the optimized nanoformulation developed according to the 3^3 FD was found in the range of 60.79±4.97 to 74.14±3.92 (table 4.2). The effect of factors on EE is expressed by the polynomial equation generated through the FD as shown below:

Entrapment efficiency =

62.167 + 0.2500 PC - 0.0500 T - 0.01000 SS - 0.0208 DD

The 3D response surface plots of the optimized nanoformulation and corresponding contour plots are shown in figure 4.4. The quadratic model's ANOVA analysis generated for all the three responses indicated no lack of fit (>0.05) between predicted values and experimental results, and thus the model can be used to plot the optimized design space.

4.5.3. Characterization of TPGS-SH

4.5.3.1. Characterization of TPGS-SH by FTIR

The IR spectrum of TPGS, TPHS-COOH and TPGS-SH were shown in the figure 4.5. TPGS has shown a C= O stretching vibration of the ester with higher intensity at 1739.46 cm^{-1}. The TPGS-COOH showed O-H stretching of the terminal carboxylic acid group of at 3514 cm^{-1}. Moreover, the -C=O stretching of -COOH at 1739.46 cm^{-1} is shifted to 1706 cm^{-1} that is the characteristic of amide link. In 4-ATP, the aromatic amine usually gives the strong C-N stretching band at 1274 cm^{-1} and N-H stretching of the primary amine as two peaks at 3434 and 3351 cm^{-1}. In place of two characteristic peaks of a primary amine of 4-ATP, a single stretching peak is evident at 3339.93 cm^{-1} in the spectra of TPGS-SH which is a characteristic of the secondary amine of amide link. All these observations indeed confirmed the formation of thiolated TPGS (TPGS-SH).

4.5.3.2. Characterization of TPGS-SH by NMR

The methylene protons of the polyethylene oxide region of TPGS-COOH produced triplet signals at 3.0, 2.58 and 2.52 ppm (figure 4.6) . The protons from the

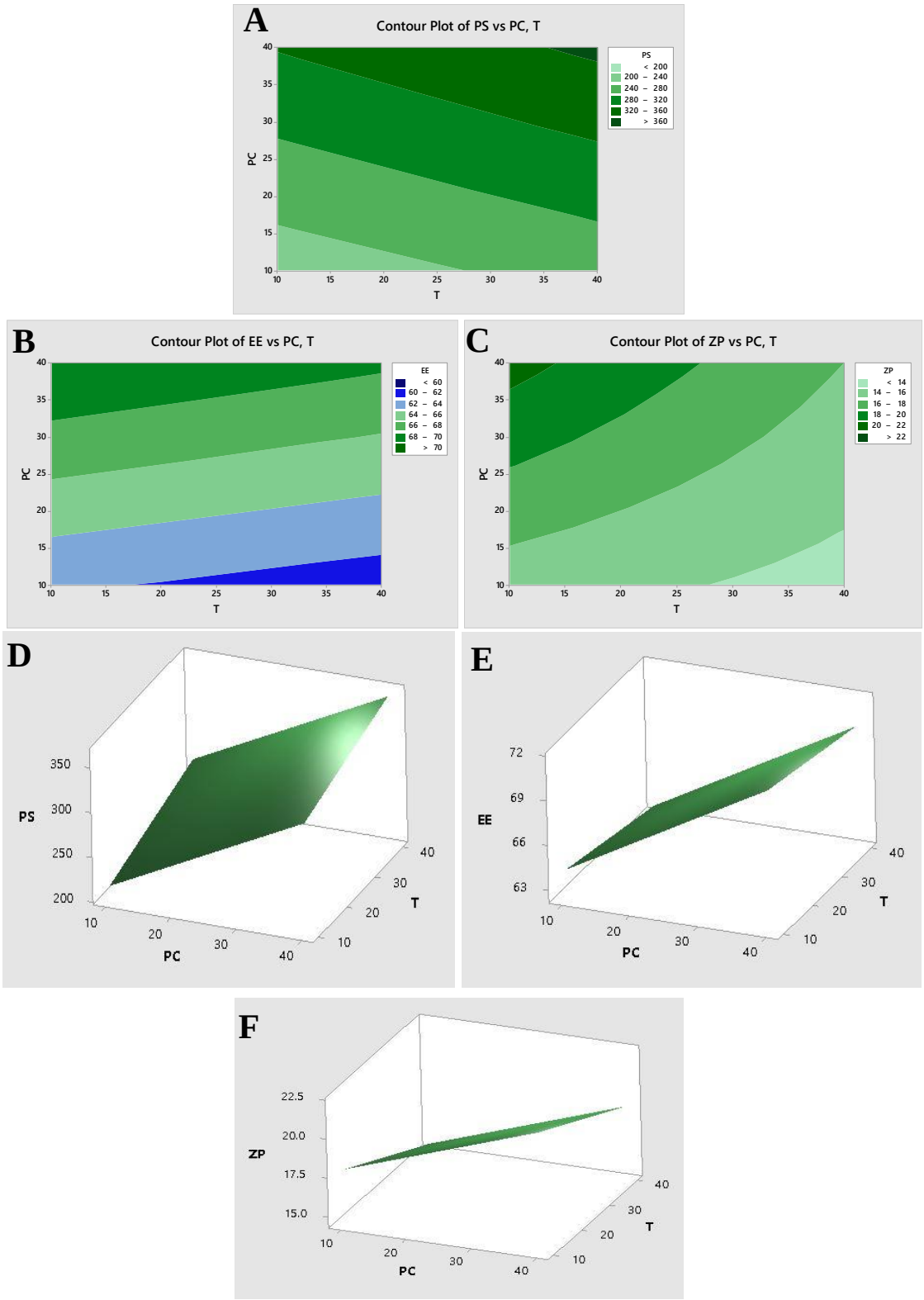

Figure 4.4. The 3D response surface plots and the contour plots showing the effect of polymer concentration (PC), temperature (T) and crosslinker concentration (CC) on particle size [A & D], zeta potential [B & E] and % entrapment efficiency [C & F].

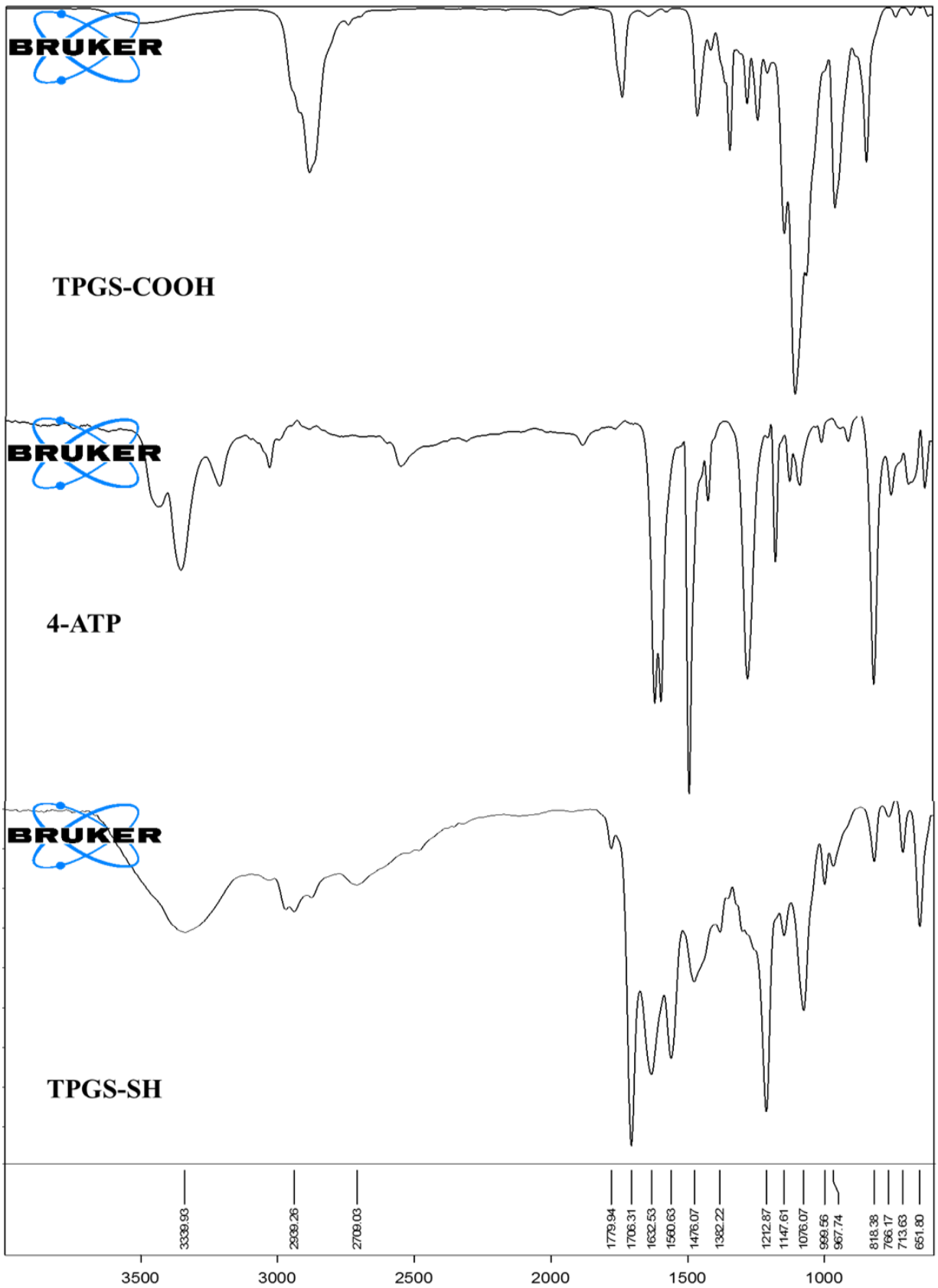

Figure 4.5. FTIR spectra of TPGS-COOH , 4-ATP and TPGH-SH

aliphatic carbon chain showed signals at 0.834 and 0.847 ppm. The peaks at 6.655, 6.668 belongs to the aromatic protons in TPGS-COOH.The two peaks observed at 3.55 and 3.59 in the spectrum of 4- ATP represent the thiol group and aromatic amino groups, respectively. The formation of TPGS-SH was confirmed by the new peak, that represents the amide link, observed at 8.09 ppm. Also, in ^{13}C NMR spectra of TPGS-SH (figure 4.6), the peak at ~174.44 ppm belongs to the -C=O group of the amide link and peak at 134.84 represents the -SH which confirmed the synthesis of TPGS-SH.

4.5.4. Physicochemical characterization

4.5.4.1. DLS analysis

The particle size and zeta potential analysis of prepared redox-sensitive nanoformulations have revealed that size and surface charge were found to be in the range of 183 to 227 nm and +18 to +26 mV (table 4.4). Surface conjugation of anti-EGFR antibody CTX has resulted a slight increase in the size of the targeted redox sensitive formulation. As the antibody CTX possesses a negative charge, its surface decoration on the targeted NP made them less positive as compared to non-targeted NP. The PDI values were also found to be within the range of 0.23±0.012 to 0.34±0.013 (table 4.4).

4.5.4.2. SEM, TEM and AFM studies

The SEM and TEM micrographs were shown in the figure 4.7 A&B. The surface morphology studies were carried out by AFM in tapping mode and the corresponding 2D and 3D micrographs were shown in figure 4.7 C&D. The SEM & TEM studies have indeed proved the uniform and spherical shape with smooth surface texture. Moreover, the particle size data from DLS measurements were found to be in absolute agreement with the size measurement data obtained from different electron microscopy studies.

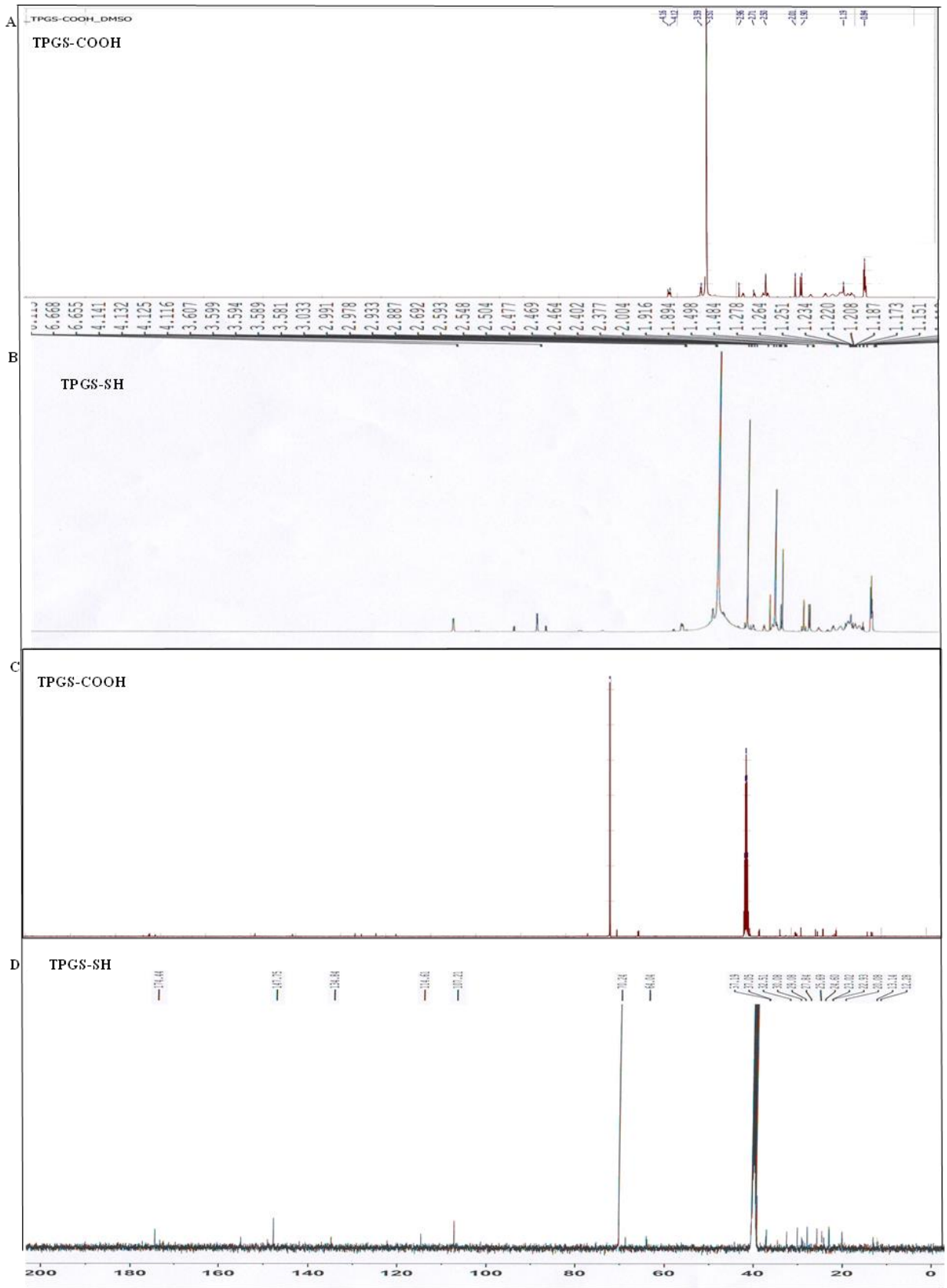

Figure 4.6. ^{1}H-NMR spectra of **A)** TPGS-COOH and **B)** TPGS-SH; ^{13}C-NMR spectra of **C)** TPGS-COOH and **D)** TPGS-SH.

The AFM analysis also revealed the even and smooth texture of the surface and the narrow size distribution of the nanoparticles.

4.5.4.3. Entrapment efficiency

The prepared non-targeted and targeted redox sensitive formulations were analyzed for the DTX entrapment efficiency and the results have shown that approximately 68% and 71% of EE was achieved, respectively (table 4.4). The beneficial interaction between the hydrophobic interior of the nanoparticles and hydrophobic DTX favored in its fairly higher entrapment. The small increment in the entrapment efficiency of targeted NP may be attributable to the surface decoration of CTX which slightly reduced the surface charge.

4.5.4.4. The extent of CTX conjugation

the amount of CTX that was attached onto the surface of targeted redox sensitive NP was determined from the Barford assay and the results have shown that nearly 72±2.179 % of CTX conjugation was achieved.

Tabel 4.4. Physicochemical evaluation parameters of different redox sensitive NP

Formulation	PS (nm)	PDI	ZP (mV)	EE (%)	T_{50} in pH 5.5, GSH 20mM (h)	T_{50} in pH 7.4, GSH 20mM (h)
Simple redox sensitive NP	183±4.496	0.23±0.012	+13±1.632	63.41±1.182		
non-targeted CM6-redox sensitive NP	187±6.944	0.27±0.016	+17±2.160	81.95±0.733	--	--
targeted CM6-redox sensitive NP	195±3.741	0.34±0.132	+14±1.247	85.57±2.276	--	--
non-targeted redox sensitive NP	204±7.408	0.31±0.028	+26±1.699	68.52±1.003	2.75	8.0
targeted redox sensitive NP	227±8.219	0.29±0.020	+22±1.054	71.08±1.016	2.52	7.2

PS- Particle size
PDI-Polydispersity index
ZP- Zetapotential
EE- Entrapment efficiency
T_{50}-Time taken for the release of 50% of entrapped drug

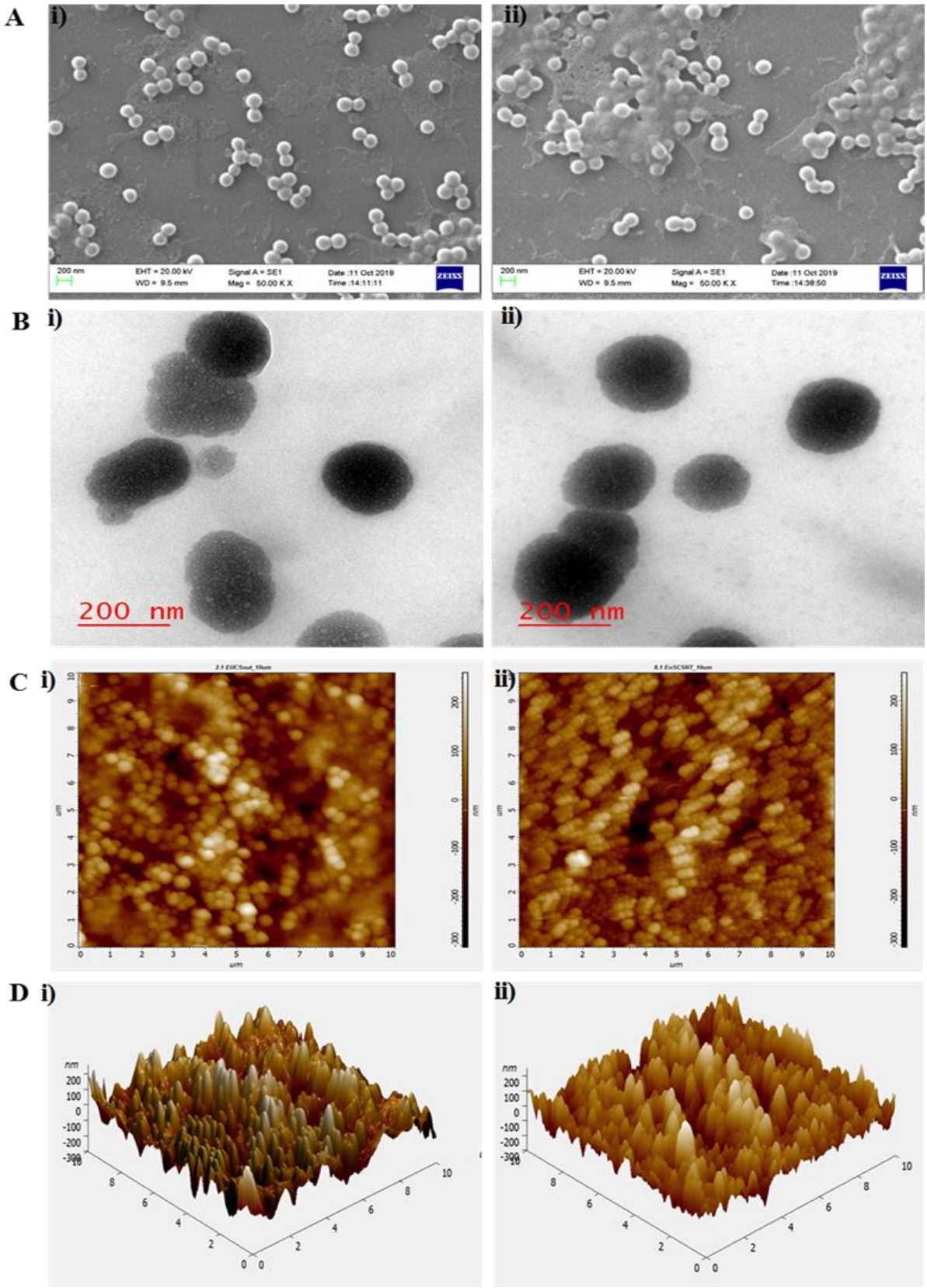

Figure 4.7. A) SEM micrographs, **B)** TEM micrographs, **C)&D)** 2D and 3D AFM images of non-targeted and targeted redox sensitive nanoparticles

4.5.5. In-vitro studies

4.5.5.1. Drug release study

The drug release was studied for 24 h at pH 5.5 and pH 7.4 with three different GSH levels i.e., 5, 10 and 20 mM and the resulting graphs were depicted in figure 4.8. The extent of drug release was found to be 39.5%, 71.4% and 91.8% for non-targeted TPGS-SH NP and it was 44.6%, 75.1% and 94.5% for targeted NP at 5,10 and 20 mM GSH concentrations, respectively within 24 h at pH 5.5. Also, At pH 7.4, the cumulative drug release after 24 h was 48.3%, 54.1% and 60.7% for non-targeted and 50.7%, 58.9% and 64.6% for targeted redox sensitive NP at 5, 10 and 20 mM GSH concentrations respectively. Drug release was found to be faster at higher GSH concentrations. Indeed, it is a well-known fact that the cancer cell microenvironment usually possesses lower pH and abnormally higher GSH levels which is nearly three times higher than that of normal cells. Interestingly, drug release was higher at lower pH 5.5, compared with that of pH 7.4. At higher pH conditions, a maximum of 64.6% of drug release was observed even with 20 mM GSH concentration, which was significantly lower than that of observed at pH 5.5. At higher pH and lower GSH levels, drug release was found to be diffusion dependent and controlled by the extent of swelling of NP. At higher GSH levels, the mechanism of drug release was principally based on the extent of degradation of NPs due to increased breakage of disulfide bonds, which was also favored by enhanced solubility and diffusion of DTX at lower pH.

4.5.5.2. pH/redox sensitivity of nanoparticles

The pH/redox sensitivity of prepared NP was ascertained by studying the changes in the particle size following 24 h incubation at various pH and GSH concentrations. At lower GSH concentrations, an increase in the diameter was noted at pH 7.4 compared to that of

at pH 5.5. Also, at higher GSH concentrations, particle size was decreased at all pH. The reason may be at higher pH, the particles may undergo considerable swelling by solvent diffusion due to increased interaction and ionization of residual surface COOH groups with the medium at lower GSH concentration. As the GSH concentration is increased, the degradation of particles may occur predominantly due to breakage of disulfide bonds, leading to a decrease in the particle sizes.

4.5.5.3. Qualitative cellular uptake study

The *in-vitro* cellular uptake studies of CM6 loaded redox sensitive TPGS-SH NP and free CM6 were conducted on A549 cell lines and the respective fluorescent micrographs are depicted in figure 4.9.A. As seen from these images, the fluorescence intensity produced by A549 cells treated with CTX decorated and CM6 loaded targeted redox sensitive NP was significantly higher as compared to that of non-targeted NP and free CM6 because of the enhanced uptake by receptor-mediated endocytosis. Also, cells pretreated with CTX have shown considerably low florescence after incubation with targeted redox sensitive NP as all the EGFR were bound with CTX and thus unavailable to facilitate endocytosis.

4.5.5.4. Cytotoxicity study

The cytotoxicity produced by both the redox sensitive NP in relation to Docel^{TM} was evaluated in the A549 lung cancer cells following their incubation with cells for 24 h at 37 ℃ and the results are depicted in figure 4.9.B. The results revealed that both the non-targeted and targeted redox sensitive NP have produced significantly higher cytotoxicity than Docel^{TM}, which was also evident from their respective IC_{50} values. The reason may be the synergism offered due to EGFR mediated ameliorated uptake of targeted NP and intracellular redox-dependent faster degradation and quick release of drug payload.

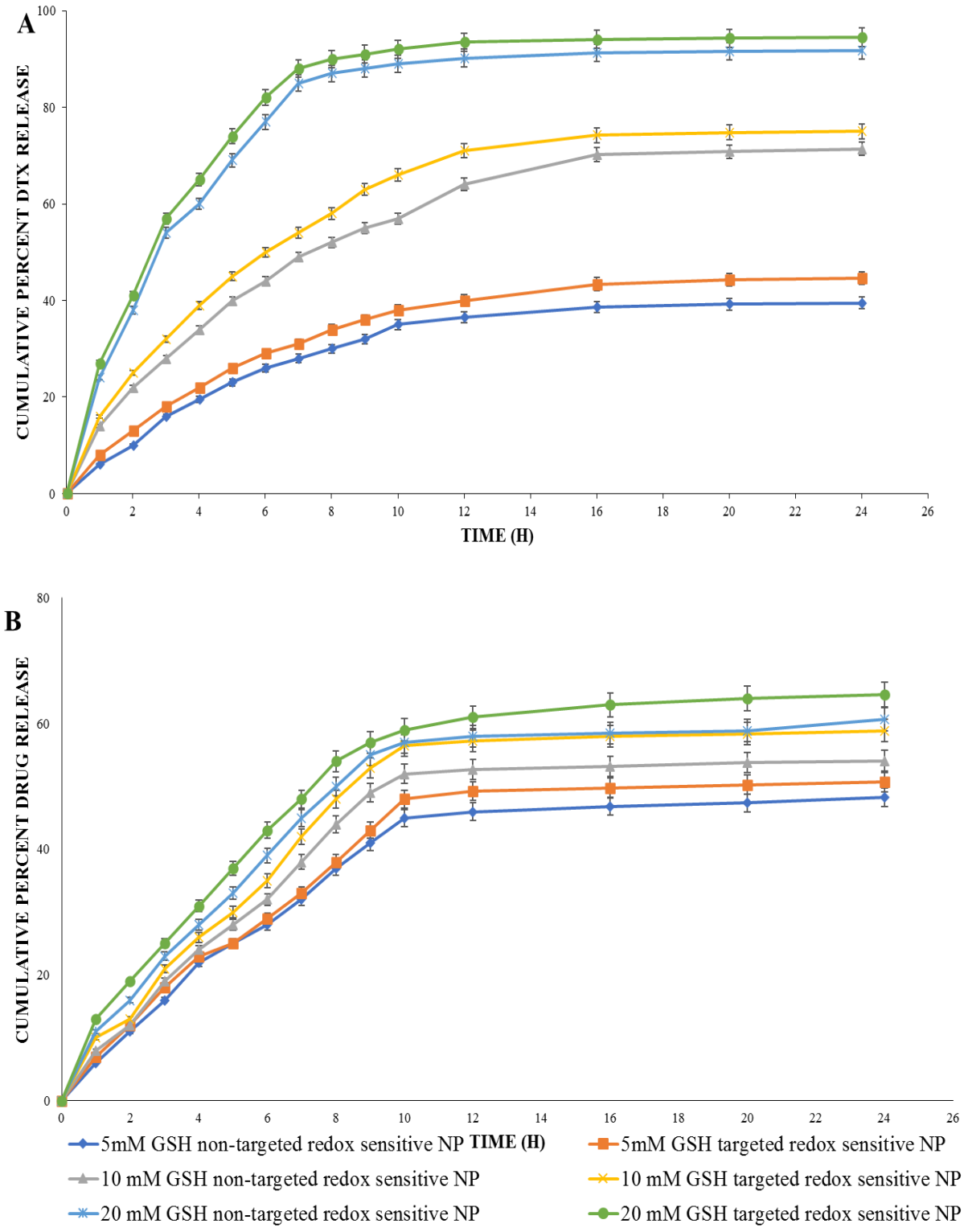

Figure 4.8. *In-vitro* drug release study in media containing different GSH concentrations in **A)** pH 5.5 and **B)** pH 7.4 buffer

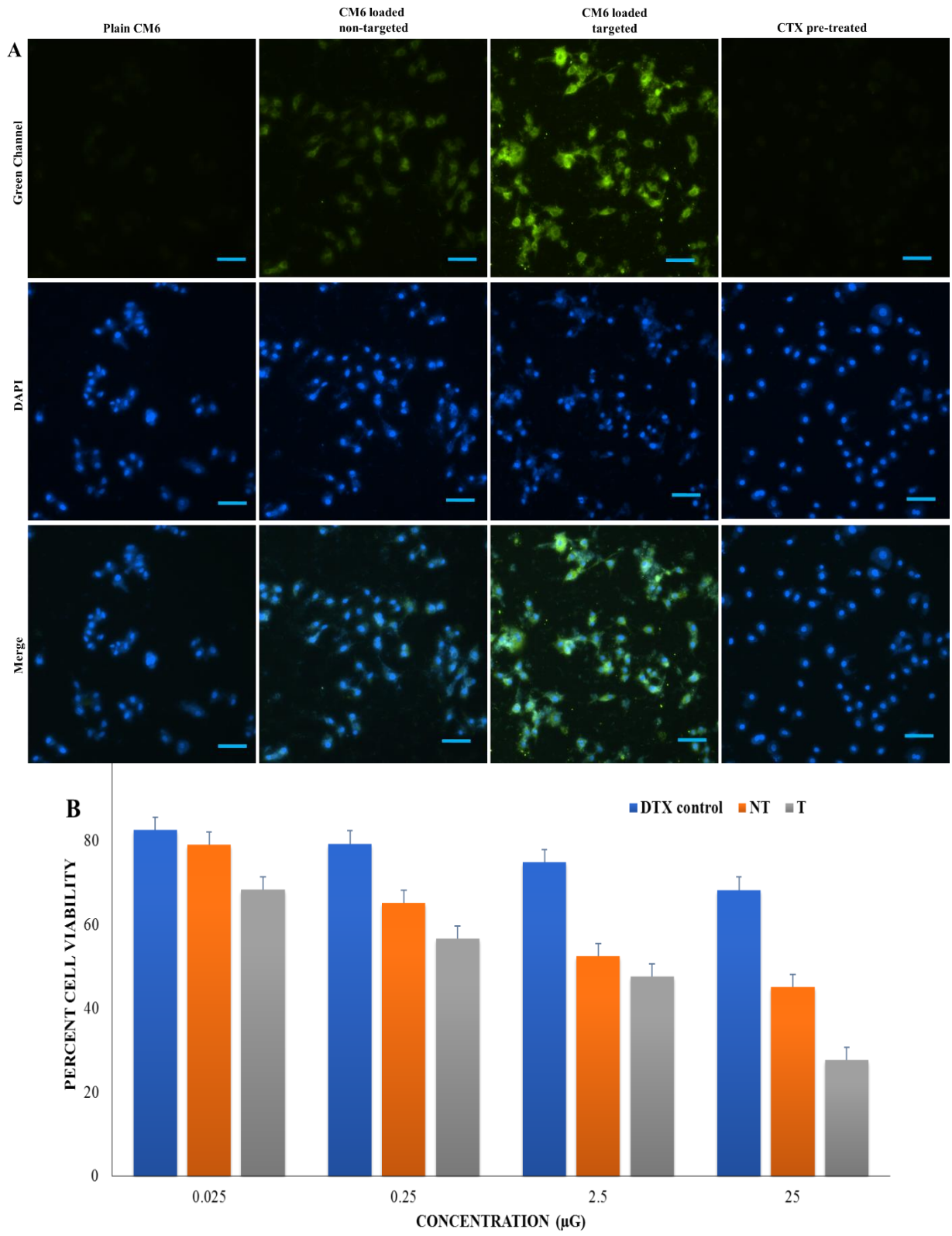

Figure 4.9. A) fluorescence microphotographs of A549 cells treated with plain CM6, CM6 loaded non-targeted and targeted redox sensitive TPGS-SH nanoparticles following counterstaining with DAPI; **B)** *in-vitro* cytotoxicity assay of Docel^{TM}, non-targeted and targeted redox sensitive TPGS-SH NP in A549 cell lines at different concentrations of DTX

Also, TPGS, being a potent inhibitor of p-GP pump, enhanced the intracellular accumulation DTX, which improved the cytotoxicity. The non-targeted NP also displayed considerable cytotoxicity as compared with the Docel^{TM} due to their redox sensitivity.

4.5.5.5. Wound healing assessment

The cytotoxic property of redox sensitive NP was ascertained by the extent of wound healing and the brightfield images are depicted in figure 4.10.A. The scratch made in the wells treated with saline control was almost covered by cells within 48 h. On the contrary, the wells treated with redox sensitive NP, no migration of cells was observed in the scratch area and interestingly, the scratch area was increased possibly due to the death of cells. The reason may be the enhanced cytotoxicity caused by the augmented drug release in presence of high redox environment of cancer cells which quickly cleaved the disulphide back bone of the TPGS-SH NP.

4.5.5.6. In-vitro apoptosis assay

The extent of apoptosis caused by DTX loaded redox sensitive formulations in comparison to Docel^{TM} was evaluated in terms of change of cellular morphology post-treatment in this study. The fluorescence micrographs of treated A549 cells after staining with DAPI and counterstaining with F-actin are shown in figure 4.10.B. As evident from the images, the cells incubated with PBS control revealed intense fluorescence in both blue and red channels with no major change in morphology. Contrastingly, huge change in morphology in the form of extensive chromosomal condensation and nuclear fragmentation was observed in the cells treated with targeted redox sensitive formulation which was higher than that caused by non-targeted NP and Docel^{TM}. The high redox-based hastened DTX release following CTX assisted augmented endocytosis of NP in

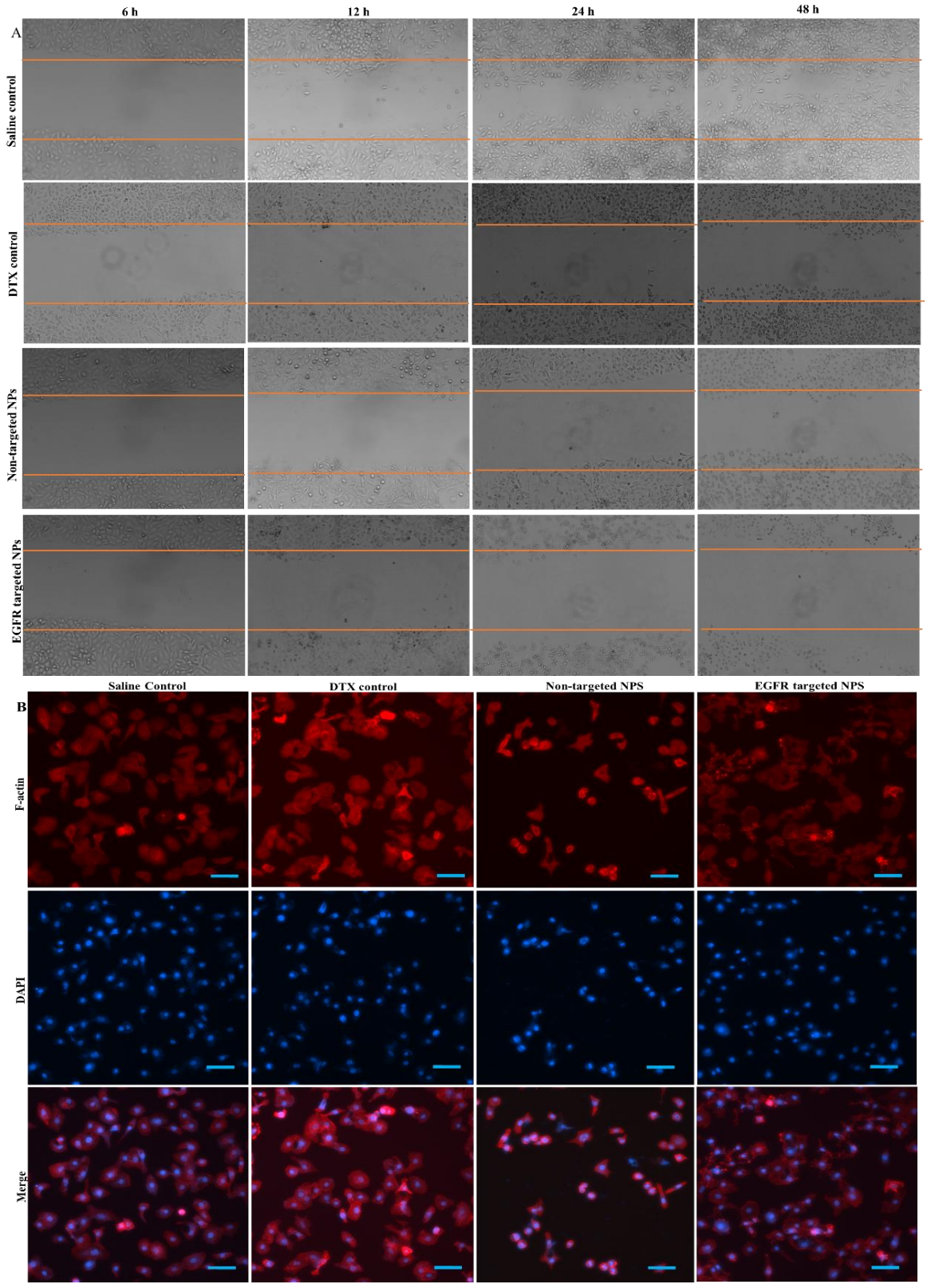

Figure 4.10. A) Brightfield microscopy images showing extent of migration of and **B)** fluorescent images of *in-vitro* morphology assay on A549 cells following treatment with saline control, Docel^{TM}, non-targeted and targeted redox sensitive nanoparticles

addition to suppression of cell membrane bound p-GP pump together constitute the potential reasons behind this superior apoptotic potential of targeted NP.

4.5.6. Stability studies

The prepared redox sensitive TPGS-SH NP were subjected to lyophilization, plasma and serum incubation and storage at 4 ℃ for six months and analyzed for stability in terms of change in particle size, zeta potential, PDI and entrapment efficiency. The results are depicted in figure 4.11. These studies have shown that the particle size and other parameters did not show significant variations post lyophilization and reconstitution as well as plasma and serum incubation and storage for six months. Usually, freeze-dried nanoformulations do sport better stability profiles since no agglomeration among the particles is possible. From the graph 4.11.A, a slight decrease in the particle size ($p\sim0.375$) and zetapotential ($p\sim0.0705$) of formulations can be noticed; a suitable explanation may be the removal of all the molecular water of hydration by lyophilization. Also the incubation with plasma has resulted in an insignificant increase ($p\sim0.0698$) in the particles sizes (figure 4.11.B) which may be due to the apparent opsonization of proteins of plasma onto the surface of NP. From figure 4.11.C, it is conspicuous that incubation with serum has no significant influence on the stability of redox sensitive NP. Nanoformulations in suspension form usually have problem with stability since with time, the chances of agglomeration of particles are increased. On the contrary, lyophilized NP will remain stable on storage for longer periods since water is not available to support microbial growth and unwanted chemical alterations. The same is evident from the figure 4.11.D, which explains that no significant variation in the particle size of NP or other parameters is noticed on storage for six months, revealing the excellent stability profile of prepared NP.

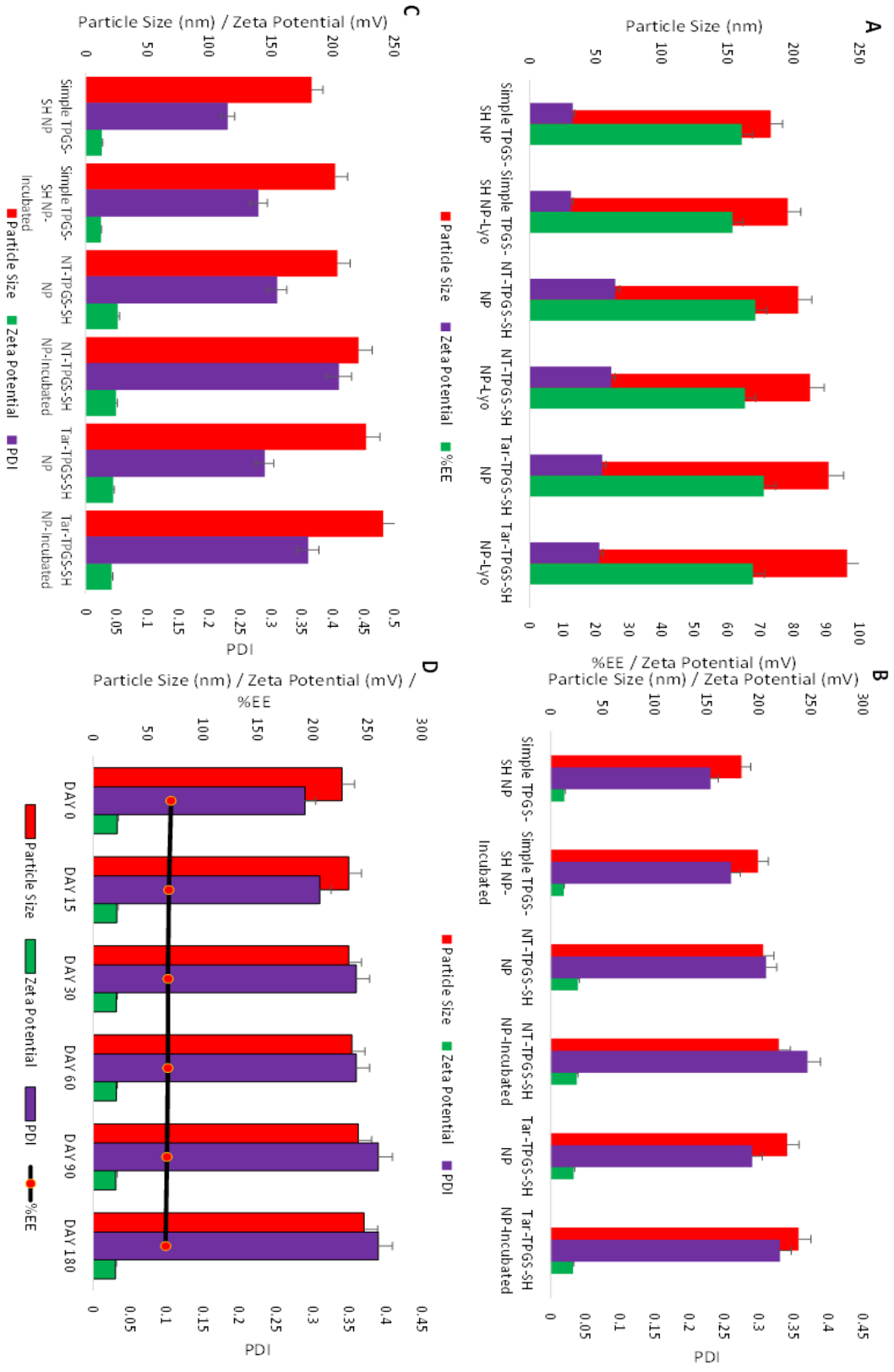

Figure 4.11. *In-vitro* stability studies particle size, zeta potential and PDI before and after **A)** lyophilization; **B)** incubation with plasma; **C)** incubation with serum; **D)** effect of storage on the stability of targeted redox sensitive TPGS-SH nanoparticles

4.5.7. In-vivo studies

4.5.7.1. Pharmacokinetics evaluation

The prepared redox sensitive non-targeted and EGFR targeted redox sensitive NP, along with Docel™, were injected to CF rats; plasma concentration Vs. time curve was constructed (figure 4.12.A) and the same was evaluated for numerous pharmacokinetic parameters using Kinetica® software. The results are tabulated in table 4.5, which showed a tremendous increment in all the pharmacokinetic parameters for redox sensitive formulations in contrast to the Docel™. There is 2.11 and 3.43 times increment in half-life, 2.526 and 4.637 times increment in relative bioavailability were observed in comparison to Docel™. There also a significant improvement in Vd and MRT was evident. The possible explanation is that the PEG portion of the TPGS-SH molecule confers stealth property to redox sensitive NP so that the formulation can evade the reticuloendothelial system, enhancing the plasma circulation as well as residence time and NP accumulation at the target site.

4.5.7.2. Histopathology studies

In an attempt to establish the safety towards vital organs, the prepared redox sensitive formulations along with Docel™ were injected to CF rats three times (7.5mg/kg) with three days interval and on the fifteenth day, the vital organs were extracted and histopathological evaluation was carried out after H&E staining. The images are shown in figure 4.12.B. From these images, it can be noticed that the non-targeted and targeted redox sensitive NP elicited insignificant toxicity to heart, lung liver and kidney tissues in comparison to that caused by Docel™.

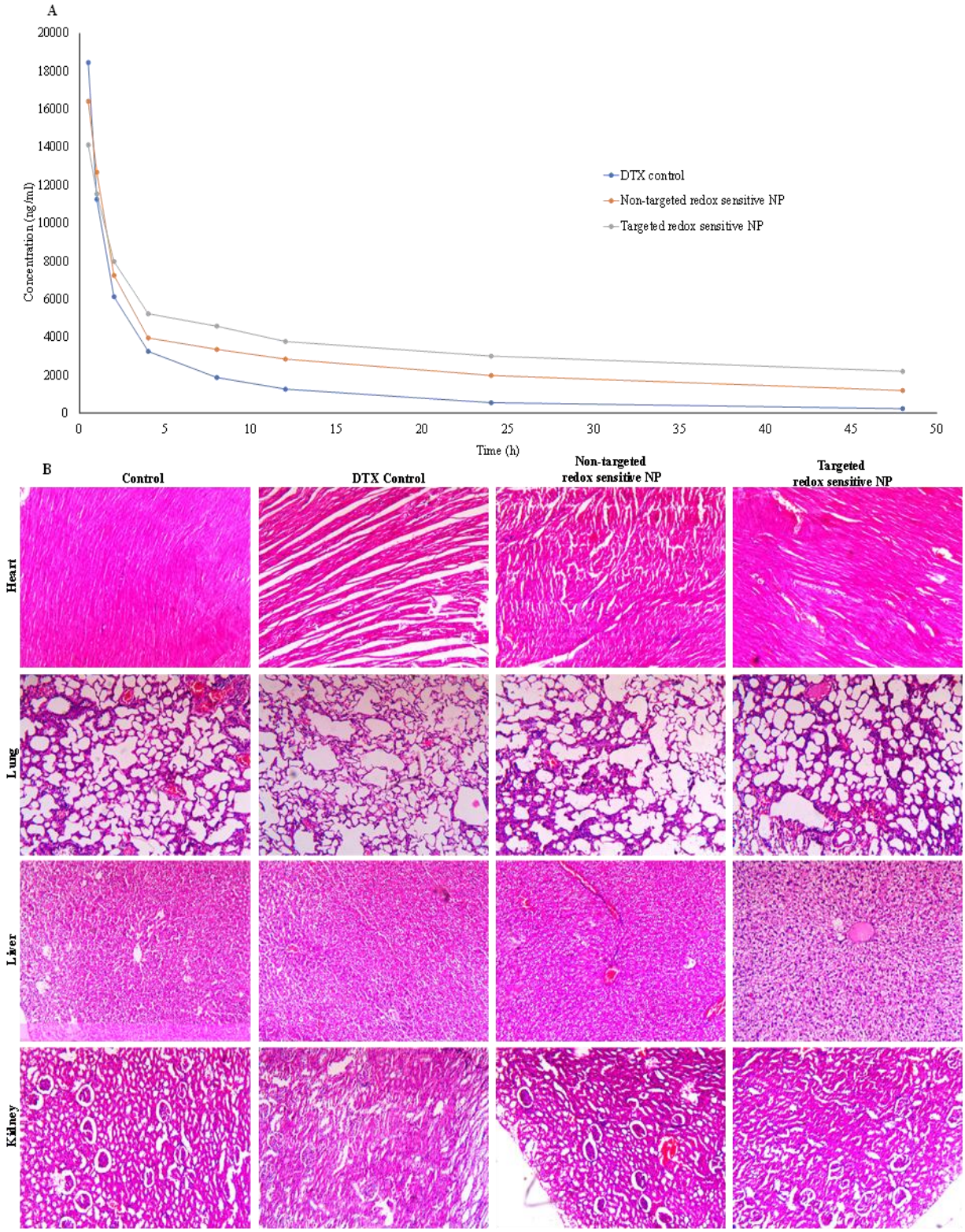

Figure 4.12. A) Plasma level-time profile after i.v. administration of the formulations; **B)** H&E stained images from histopathological evaluation of vital organs such as heart, lung, liver and kidney after i.v. administration Docel™, non-targeted and targeted redox sensitive TPGS-SH NP

It is a well-known fact that TPGS is considered as GRAS material by FDA which establishes the safety of TPGS and its conjugates. The same is indeed approved from the above histopathological evaluation in which no sign of pathological changes was seen in the vital organs.

Table 4.5. Pharmacokinetic parameters of non-targeted and targeted redox sensitive TPGS-SH NP

Pharmacokinetic parameter	Docel™	Non-targeted redox sensitive NP	Targeted redox sensitive NP
$t_{1/2}$ (h)	13.734±0.5301	29.07±0.8563	47.11±0.9883
K_E (/h)	0.5045±0.031	0.0238±0.001	0.0147±0.001
AUC_{tot} (ng.h/ml)	68733±2489	173621±2776	318760±5041
MRT (h)	13.437±0.854	37.29±1.2581	63.91±1.853
V_d (l/kg)	0.2163±0.015	1.812±0.121	1.6±0.092
CL_t (l.kg/h)	0.1091±0.011	0.04317±0.003	0.02353±0.001
AUC_{0n} (ng. h/ml)	70761±1513	144138±1736	175285±1911
F_R	--	2.526±0.192	4.637±0.24

4.5.7.3. In-vivo anticancer efficacy of redox sensitive TPGS-SH NP

The ImageJ® processed images of H&E stained histological sections of benzo(a)pyrene-induced NSCLC after treatment with saline control, Docel™, non-targeted and targeted redox sensitive NP are depicted in figure 4.13, in which, model control showed the well-differentiated adenocarcinoma with multifocal origin from the bronchioles. The cells have been presented with characteristic polygonal appearance with large spherical or sometimes oval and vesicular nuclei and vacuolated and scanty cytoplasm. Here, a feature of ImageJ software named ‘color deconvolution’ was used to separate the nucleus from cytoplasm for further quantitative evaluation of lung cancer after treatments. Following treatments for the specified time, the H&E sections were analyzed by ImageJ® software by selecting six different areas from each color deconvoluted image and counting the number of particles (nuclei).

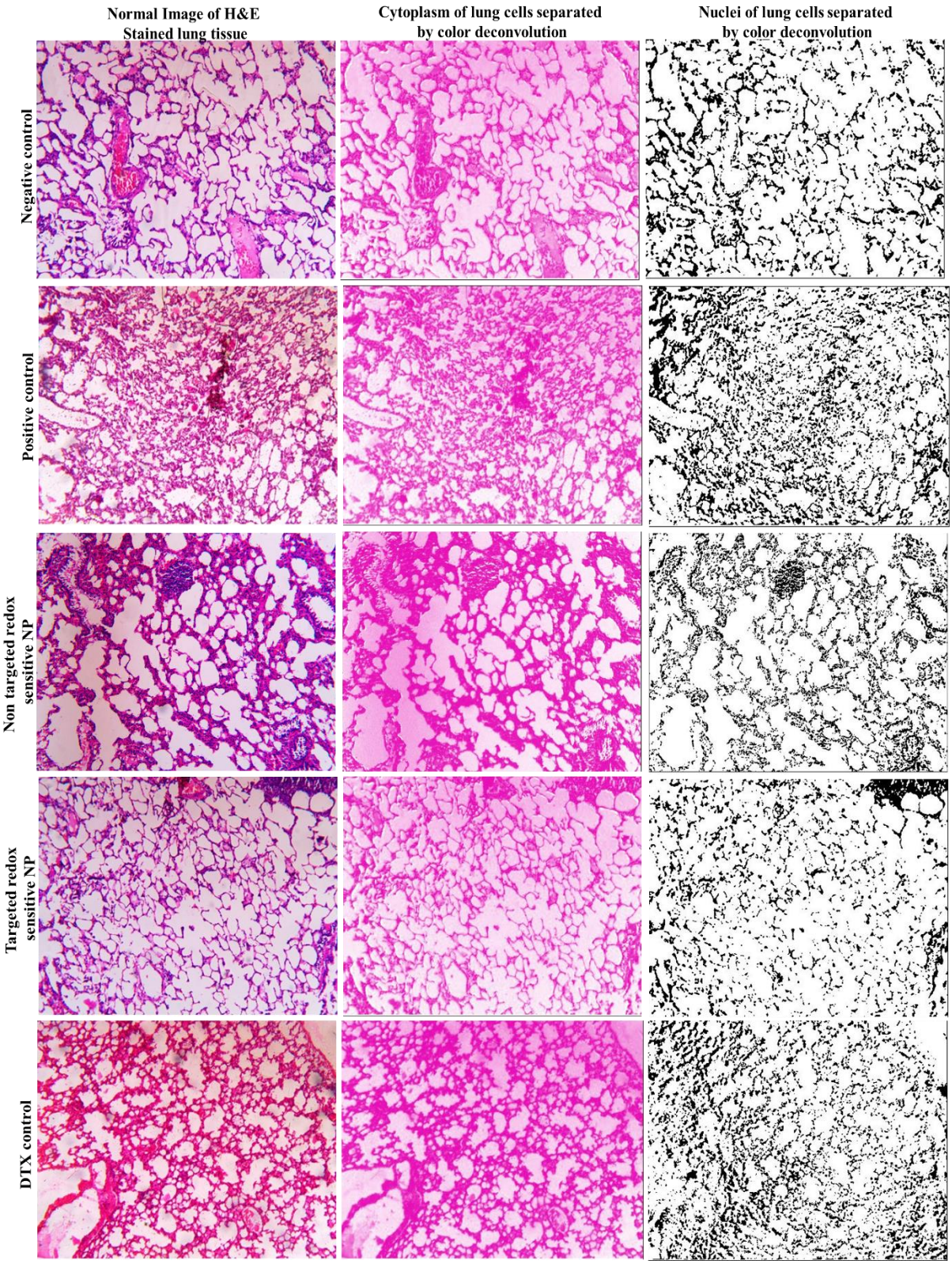

Figure 4.13. Colour deconvoluted images of the H&E stained histological sections of lung cancer tissues by ImageJ® after treatment with control, Docel™, non-targeted & targeted redox sensitive TPGS-SH formulations

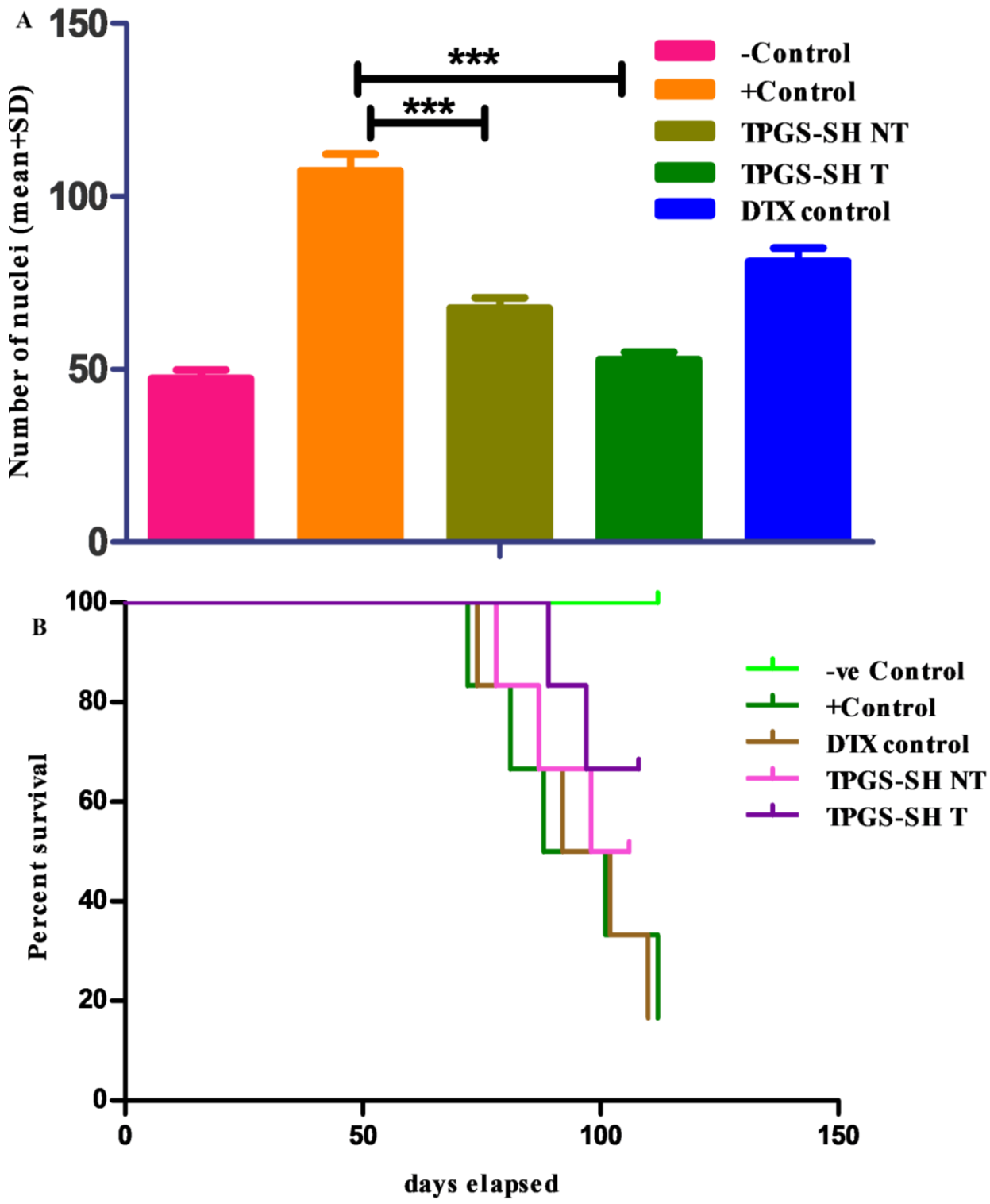

Figure 4.14. A) Graph showing the comparative *in-vivo* tumor inhibition by Docel™, non-targeted and targeted redox sensitive TPGS-SH formulations in comparison to saline control and Model control. (***P<0.0001, *P<0.05), **B)** Kaplan-Meier survival analysis of mice treated with negative control, model control non-targeted and targeted redox sensitive TPGS-SH formulations and Docel™

One way ANOVA was used to arrive at statistically meaningful comparisons. The typical values are depicted in figure 4.14.A, which established that a significant reduction in the cell number and tumor growth was caused by non-targeted and targeted redox sensitive NP in comparison to Docel^{TM} and, all the treatments have significantly reduced the tumor number in contrast to model control. Also targeted TPGS-SH NP ($p<0.001$), compared to the non-targeted, caused a significant reduction in cancer cell numbers. Even non-targeted TPGS-SH NP also showed comparable efficacy ($p<0.05$) as they also possess the advantages of EPR effect and presence of amorphous form of drug embedded in the biodegradable matrix.

The Kaplan-Meier survival analysis was done to evaluate the mean survival rate of the B(a)P induced lung cancer mice post-treatments and the same is depicted in figure 4.14.B, which showed that the percent survival of B(a)P mice treated with non-targeted and targeted redox sensitive formulations was significantly prolonged as compared with model control.

4.6. Conclusion

In the current research work, a novel redox sensitive TPGS-SH based anticancer nanomedicine, with and without CTX conjugation was prepared so as to establish DTX loaded and EGFR targeted TPGS-SH NP for the active targeting of NSCLC. TPGS-SH was synthesized by using carbodiimide chemistry and the same was confirmed by FTIR and NMR analyses. Following, redox sensitive TPGS-SH NP were prepared by dialysis method and the formulations were evaluated for physicochemical, *in-vitro* and *in-vivo* parameters. The particle size, charge, polydispersity index and entrapment efficiency were in satisfactory limits. The *in-vitro* release was studied at pH 5.5 and 7.4 with various GSH concentrations and the results have shown that at higher GSH levels, drug release

was found to be faster which is in tune with the *in-vivo* requirement where high inherent redox potential is obvious (>20 mM) at cancer microenvironment. The pH and redox sensitivity studies also established the same fact that at acidic pH, particle size was found to be low due to degradation of disulfide bonds with high GSH concentration and at higher pH, particle size was increased due to swelling at lower GSH levels. *In-vitro* cellular uptake studies proved the enhanced uptake of CM6 loaded CTX decorated redox sensitive NP in comparison to free CM6 and non-targeted NP. *In-vitro* cytotoxicity, wound healing and *in-vitro* morphology assays also proved the superiority of targeted NP. The *in-vitro* stability studies also revealed that prepared targeted formulations were sufficiently stable. *In-vivo* pharmacokinetic studies have shown that prepared formulations achieved higher plasma circulation times and relative bioavailability as compared with the Docel™. *In-vivo* histopathologic evaluation of vital organs confirmed the safety of the redox sensitive NP towards the heart, liver, lungs and kidney. *In-vivo* tumor inhibition studies on B(a)P induced lung cancer sections of mice that were processed with ImageJ® have also stated that cell number was reduced significantly by targeted redox sensitive NP as compared with non-targeted NP and both the formulations have demonstrated superior anti-cancer effect than Docel™. In conclusion, this novel redox sensitive TPGS-SH nanomedicine can be a promising platform for the delivery of antineoplastics after the proper further clinical validation.